Graphene nanoribbons

Ultralong Natural Graphene Nanoribbons and Their Electrical Conductivity**

Miriam Moreno-Moreno, Andrés Castellanos-Gomez, Gabino Rubio-Bollinger, Julio Gomez-Herrero, and Nicolás Agraït**

Graphene is a 2D material with many possible applications in material science,[1] nanomechanics,[2] and nanoelectronics.[3] While high-yield production methods for graphene sheets are a hot research topic,[4–7] so far most of the experiments are performed on graphene flakes obtained by micromechanical cleavage.[8,9] As reported by a number of recent theoretical works,[10–13] graphene nanoribbons (GNRs) are expected to have new properties with respect to graphene flakes. However, experimental work related to GNRs is not so abundant. GNRs have been produced by lithographic technique[14–16] or by chemical procedures,[17–20] but to our knowledge they have been never been obtained by micromechanical cleavage. This method presents some advantages over other methods, for example, electron-beam lithography may produce ill-defined edges and chemical synthesis involves a quite sophisticated preparation.

We introduce a simple method for graphene-flake deposition based on silicone stamps. Using optical and atomic force microscopy (AFM), we characterize the flakes, finding ultralong GNRs with a minimum width below 20 nm that are electrically characterized by conductance AFM. As the ribbons are a consequence of the cleaving process (natural GNRs), we expect clean edges along the crystallographic graphene directions and low defect density.

Graphene is a single layer of graphite and consequently it can be considered an almost ideal 2D material. Many of the exotic properties measured in graphene[21–24] are a direct consequence of this low dimensionality and the relativistic-like behavior of its charge carriers. This introduces a new kind of property that cannot be found in other materials. When a graphene flake is reduced to a long nanometers-wide ribbon, additional properties emerge in the already rich scenario of graphene. In particular, lateral confinement of the charge carriers causes the opening of an energy gap, which depends on the width of the nanoribbon.[13,14,25] Crystallographic orientation has been predicted to play a key role, as in the case of carbon nanotubes, in the electrical properties of GNRs. Graphene flakes obtained by micromechanical cleavage show well-defined edges naturally produced during the cleaving process. For the case of GNRs obtained by lithographic technique, this is unclear and one may expect to have ill-defined edges. State of the art lithography has a resolution of about 10 nm and this imposes a limit for defining GNR edges. Further complications could arise from the fact that lithography techniques may contaminate the sample and in particular the edges of the GNR.[26,27] A new procedure to obtain GNRs was recently presented by Xiaolin Li et al.[17] The authors report submicrometer-length nanoribbons with a minimum width below 10 nm. The ribbons are obtained through a complicated chemical process that can be also used (with small variations) to produce graphene flakes. Although the graphene flakes produced by the chemical route are of good quality, they are still far from the ones prepared by mechanical cleavage. This may also happen for chemically obtained GNRs.

Our samples are prepared by a variation of the transfer printing technique.[28] Poly(dimethylsiloxane) (PDMS) stamps, commonly known as silicone stamps, are used to cleave highly oriented pyrolytic graphite (HOPG). Cleaved graphite is then transferred to an insulating surface to make electrical transport measurements possible. The microcleaving speed was not measured with accuracy but we have noticed that it plays a relevant role to obtain good quality samples.[28] As a reference, in our preparation it takes 5 to 10 s to peel the stamp. The substrate was previously cleaned by sonication in acetone (5 min) followed by a short heating in air to completely remove the acetone from the surface. We chose

[*] Prof. J. Gomez-Herrero, Prof. G. Rubio-Bollinger
Departamento de Física de la Materia Condensada and
Instituto Nicolás Cabrera
Universidad Autónoma de Madrid
28049 Madrid (Spain)
E-mail: julio.gomez@uam.es
Prof. N. Agraït
Departamento de Física de la Materia Condensada
Instituto Nicolás Cabrera and
Instituto Madrileño de Estudios Avanzados en
Nanociencia IMDEA-Nanociencia
Universidad Autónoma de Madrid
28049 Madrid (Spain)
E-mail: nicolas.agrait@uam.es
A. Castellanos-Gomez, M. Moreno-Moreno
Departamento de Física de la Materia Condensada (C-III)
Universidad Autónoma de Madrid, 28049 Madrid (Spain)

[**] We would like to thank M. Vélez for introducing us to the PDMS stamp fabrication technique and B. J. Basilio for the oxidation of our silicon wafers. This work was supported by MEC (Spain) (MAT2007-66476-C02-01, MAT2004-03069, and NAN2004-09183-C10-05/06), MICINN (Spain) (MAT2008-01735 and CONSOLIDER-INGENIO-2010 CSD-2007-00010), and Comunidad de Madrid (Spain) through programs NanoObjects and Citecnomik (S-0505/MAT/0303, S_0505/ESP/0337).

DOI: 10.1002/smll.200801442

a 285-nm-thick layer of thermally grown silicon oxide as an isolator to facilitate optical characterization of graphene.[29] A highly *p*-type-doped silicon substrate allows electrical characterization of the sample even at low temperatures. The use of PDMS stamps, instead of the commonly used Scotch tape, avoids traces of glue over the surface during the graphite transfer process.

The essential step in our fabrication procedure is the use of a second clean PDMS stamp to cleave the graphite flakes previously transferred on the SiO_2 surface again. Most of the graphite is removed in this way, leaving only thin graphite flakes on the surface. Figure 1 shows an example of a thin graphite flake obtained using this method. Two features can be seen at first glance: first, the well-defined crystallographic directions expected for crystalline graphite that are also characteristic of the conventional micromechanical cleavage technique using Scotch tape. Second, the flake resembles a frayed fabric. This is particularly clear in the upper side of the flake where many thin ribbons protruding from the mother flake can be seen. For instance, the wide ribbon marked with a green arrow in the optical microscope image has a width, according to the AFM image, of about 1.1 μm. Ribbons as narrow as 200 nm can be found in about one fourth of the samples characterized by optical microscopy.[29] A more detailed inspection in the vicinity of these ribbons using AFM and scanning electron microscopy reveals that in one half of the cases there are also narrower nanoribbons whose widths range between ≈20–120 nm. The use of AFM allows us to characterize the thickness of these flakes and nanoribbons that can be as thin as one monolayer. A relevant example of an isolated nanoribbon is shown in Figure 1b. The ribbon that starts in a relatively small flake has a length of about 25 μm, with an almost uniform width of 37 nm and a thickness ranging from 1 to 2 nm.

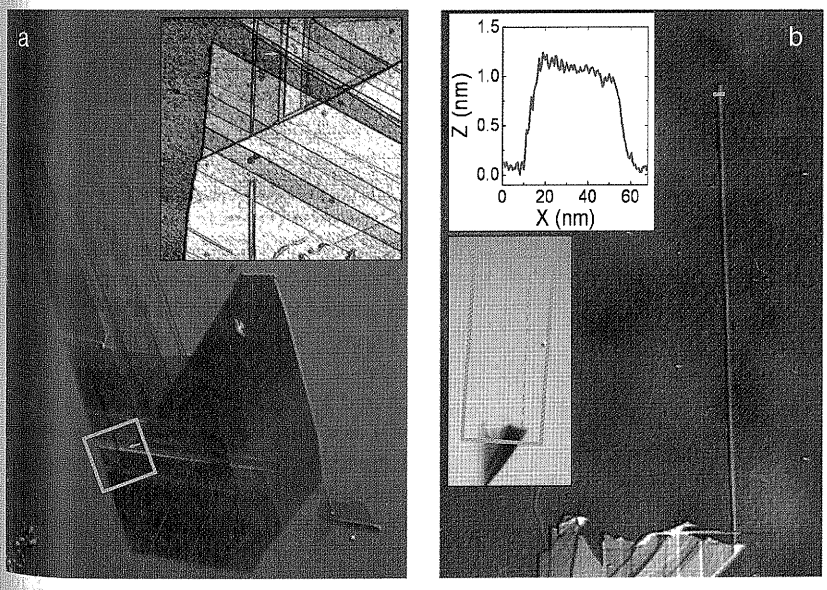

Figure 1. a) Phase contrast optical microscopy image of a graphene flake and several ribbons following its crystallographic directions. The inset is a $10 \times 10\ \mu m^2$ AFM topograph of the region enclosed by the square. The marked ribbon in the inset is 1.1-μm wide and the thinner one on the left is 150-nm wide. The former is also visible in the optical microscopy image (marked with an arrow) while the latter is hardly noticeable. As the optical microscope image shows, the sample surface is quite clean. b) AFM topography of a 37-nm-wide ribbon emerging from a graphite flake. This ribbon has a length of ≈24 μm and a thickness ranging from 1 to 2 nm. The upper inset is a profile.

After sample preparation, a 20-nm-thick gold electrode is thermally evaporated by means of a glass shadow mask for further electrical characterization. This mask covers the selected nanoribbons and partially the mother flake. Therefore, the nanoribbons are electrically connected to the gold electrode through the mother flake. In this way graphene is never exposed to chemicals as during a lithography process that can alter its electronic properties.[26,27]

Figure 2a is a composition of twelve AFM topography images showing the edge of a flake (left side of the image) and three narrow ribbons protruding from this flake. The total length of the image is about 50 μm. Figure 2b is a zoomed-in image of the previous image where the three ribbons can be seen in more detail. The profile measured along the upper green line (Figure 2c) shows ribbon heights ranging from 0.8 to 1 nm compatible with a thickness of one or two graphene layers.[17] We have taken higher magnification AFM images to accurately measure the narrowest ribbon dimension (not shown). The profile in Figure 2d belongs to one of these images and has been marked with a short green line in Figure 2b. Unfortunately, we do not have enough resolution to measure the geometry of the edge and therefore it is not possible to correlate the electrical characteristics of the nanoribbon to its structure. The AFM tip–ribbon dilation produces an unrealistic width for the profile. The width increment due to tip dilation can be estimated as $\Delta W = 2[h(2R-h)]^{1/2}$, where R and h are the tip radius and ribbon thickness, respectively.[30] For a 20-nm tip apex radius (value obtained by taking images of a reference sample with single-walled carbon nanotubes (SWNTs)) imaging a 1-nm-high flake, the dilated image width will be increased ≈12 nm. This is the same as saying that the real width of the ribbon coincides with the flat part of the profile (Figure 2d). This indicates that the real minimum width of this ribbon is below 20 nm.

The electrical characterization of the nanoribbons is carried out by means of conductance AFM. In order to obtain reliable results we use AFM cantilevers with a ≈50-nm-gold/palladium coating. To avoid tip contamination it is important to use recently covered (or kept in vacuum) cantilevers. In our experimental setup, the metalized AFM tip is used to measure the current versus voltage (I–V) characteristics (Figure 3c) of the nanoribbons as a function of the distance between the metallic AFM tip, used as mobile electrode, and a fixed macroscopic gold electrode.[31] A highly doped silicon substrate allows us to apply a backgate in our measurements (inset Figure 3a). Briefly, the experiments are performed as follows: a nanoribbon is first selected (Figure 2) and then electrically

characterized. From a linear fit of the *I–V* characteristics (Figure 3c) at zero bias voltage, the electrical resistance is determined along the nanoribbon at a fixed backgate voltage (Figure 3a). The experimental setup enables us to increase the force applied on the nanoribbon by the mobile electrode, until an optimum contact resistance is reached. For SWNTs, the mechanical load applied to measure the *I–V* curves is a key factor to determine the electrical resistance of the nanotube.[32] For low mechanical loads a tunnel barrier is present between the tip and the nanotube, and the electrical resistance is quite high. As the tip presses the nanotube, the tunnel barrier and the electrical resistance drop until an optimum contact is reached.[32] If the mechanical load is further increased, the SWNT is deformed, changing its band structure, which is reflected on a bandgap opening. Using conductance AFM, optimum resistances of almost 6.5 kΩ (the minimum possible resistance for a SWNT) have been reported.[33] The results obtained using conductance AFM are in excellent agreement with those obtained using more conventional techniques. For instance, the room temperature 1D electrical resistivity obtained by using an array of nanoelectrodes along metallic SWNTs[34] is $\rho_{1D} = 11\,k\Omega\,\mu m^{-1}$, while using conductance AFM we obtained an average 1D resistivity for eight different SWNTs of $\rho_{1D} = 10 \pm 2\,k\Omega\,\mu m^{-1}$ (see gray dashed line in Figure 3a).[35] For the case of the nanoribbons, we observe a contact improvement at low mechanical loads. This suggests, as for nanotubes, the presence of a tunnel barrier, but once the electrical contact is optimized we have never observed any dependence of the electrical resistance with the mechanical load. Besides, our experiments do not show any particular correlation between the flake thickness and the electrical contact resistance that varies from 1.5 to 4 kΩ for thicknesses ranging from 0.8 to 17 nm and a common backgate of 0 V, confirming the low out-of-plane conductance of graphite.[36] For all the measurements, we first check the tip state by contacting it with the gold electrode; we consider a tip as acceptable when the measured electrical resistance is lower than 2 kΩ.

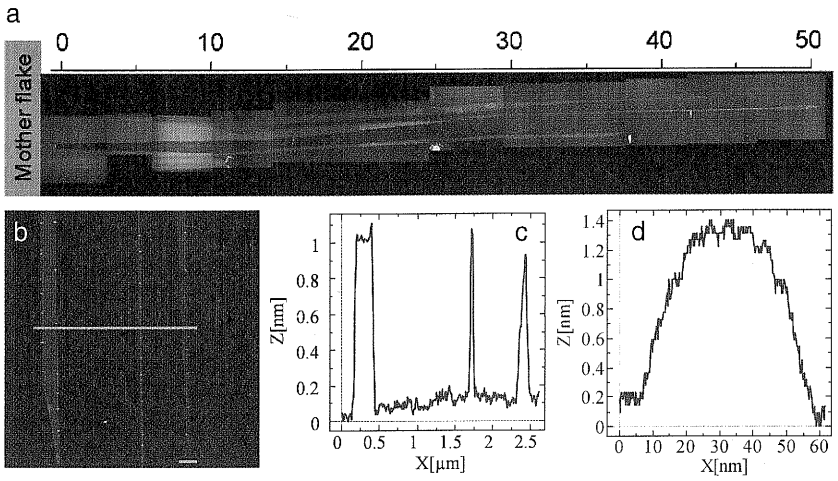

Figure 2. a) Composition of twelve AFM topography images showing three nanoribbons. The upper scale shows the length in micrometers. b) 4 × 4 μm² AFM topograph showing a detailed view of the three nanoribbons. c) Profile along the upper green line showing the height and width of the nanoribbons. d) Profile along the lower green line showing the minimum width of the nanoribbons.

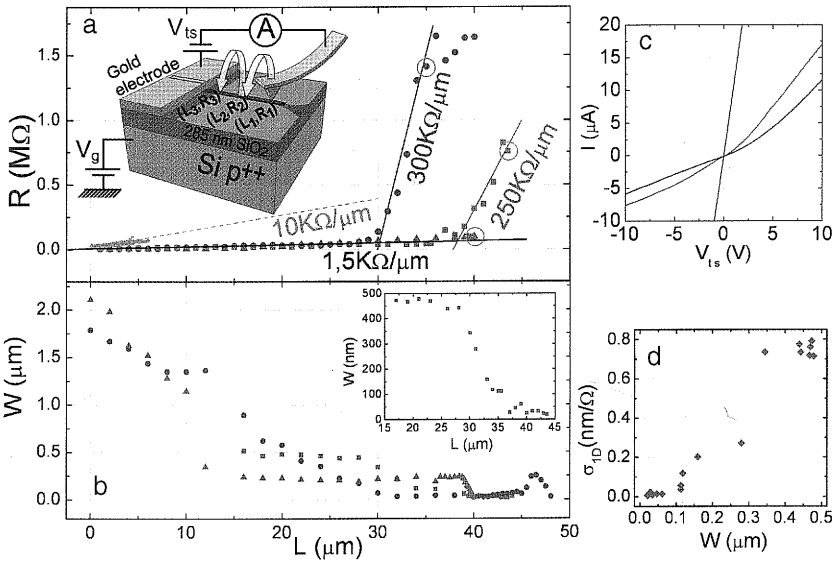

Figure 3. (a) and (b) show the low voltage resistance and width, respectively, of nanoribbons RA (green squares), RB (blue circles), and RC (red triangles) as a function of distance to the mother flake. The slope of the resistance (or 1D resistivity, $\rho_{1D} = dR/dL$) is fairly constant at large distances from the mother flake. The experimental $R(L)$ of eight different metallic SWNTs [35] has also been plotted for comparison (gray). The inset in (a) illustrates the experimental procedure. At each position of the conducting tip in the nanoribbon, the current versus tip-sample bias (V_{ts}) voltage characteristic is measured and the low voltage resistance is obtained from the slope at zero bias. Typical *I–V* characteristics are shown in (c). The rectifying character observed in these characteristics suggests the semiconducting behavior of the ribbons. The inset in (b) shows a zoomed-in image of the width of the thinnest part of ribbon RA. d) $\sigma_{1D} = 1/\rho_{1D}$ as a function of width for ribbon A, where σ is the 1D conductivity. The observed linear dependence is to be expected for a material with a constant sheet resistivity ρ_{2D}, since $\sigma_{1D} = W/\rho_{2D}$. From the inverse of the slope we obtain a sheet resistivity $\rho_{2D} = 500\,\Omega$.

Figure 3a shows the low voltage resistance for the three nanoribbons (denoted RA (green), RB (blue), and RC (red)) as a function of their length. Below, sharing the same horizontal axis, the widths of the three ribbons have been plotted. The 1D resistivity, $\rho_{1D} = dR/dL$, of ribbon RC is almost constant and very low ($<1.5\,k\Omega\,\mu m^{-1}$), the same magnitude for the two other ribbons grows to hundreds of $k\Omega\,\mu m^{-1}$ in the narrowest part. The correlation between 1D resistivity and width W is evidenced in Figure 3d, which shows the inverse of ρ_{1D} versus W for RA. The observed linear dependence is expected for a material with a constant

sheet resistivity ρ_{2D}, since the contribution of an element of length ΔL to the resistance of the nanoribbon would be $\Delta R = \rho_{2D}/W\Delta L$, and consequently $1/\rho_{1D} = W/\rho_{2D}$. The value obtained for the sheet resistivity $\rho_{2D} = 500\,\Omega$, far from the maximum resistivity value (Dirac point),[37] is consistent with that observed by Kim et al.[14] Our results are also compatible with the existence of an inactive width of several nanometers, although the dispersion in the data and the experimental uncertainty in the GNR width make a precise determination of the resistivity value difficult. Chemically fabricated nanoribbons also show a very similar value for the resistivity.[17] We have estimated the mobility of a 80-nm-wide and 22-μm-long GNR using a simple electrostatic model.[21] We obtain a value of $800\,cm^2\,V^{-1}\,s^{-1}$,[38] which is of the same order of magnitude of the mobility reported in references.[14,15,17]

This work is the result of an intensive but not extensive effort for the fabrication and characterization of narrow nanoribbons. We are sure that a more thoughtful search will certainly lead to even narrower nanoribbons where the effects of 1D quantum confinement shall be more accessible. Other interesting effects have also been predicted for narrow (less than ≈6 nm) GNRs with well-defined edges. For instance, spin-separation and half-metallicity in the presence of a transverse electric field with possible applications in spintronics have been predicted for zig-zag-edged GNRs.[39]

Keywords:
atomic force microscopy · conductivity · graphene · micromechanical cleavage · nanoribbons

[1] S. Stankovich, D. A. Dikin, G. H. B. Dommett, K. M. Kohlhaas, E. J. Zimney, E. A. Stach, R. D. Piner, S. T. Nguyen, R. S. Ruoff, *Nature* **2006**, *442*, 282.
[2] J. S. Bunch, A. M. van der Zande, S. S. Verbridge, I. W. Frank, D. M. Tanenbaum, J. M. Parpia, H. G. Craighead, P. L. McEuen, *Science* **2007**, *315*, 490.
[3] A. K. Geim, K. S. Novoselov, *Nat. Mater.* **2007**, *6*, 183.
[4] C. Berger, Z. M. Song, T. B. Li, X. B. Li, A. Y. Ogbazghi, R. Feng, Z. T. Dai, A. N. Marchenkov, E. H. Conrad, P. N. First, W. A. de Heer, *J. Phys. Chem. B* **2004**, *108*, 19912.
[5] C. Gomez-Navarro, R. T. Weitz, A. M. Bittner, M. Scolari, A. Mews, M. Burghard, K. Kern, *Nano Lett.* **2007**, *7*, 3499.
[6] L. Xiaolin, Z. Guangyu, B. Xuedong, S. Xiaoming, W. Xinran, W. Enge, D. Hongjie, *Nat. Nanotechnol.* **2008**, *3*, 538.
[7] Y. Hernandez, V. Nicolosi, M. Lotya, F. M. Blighe, Z. Y. Sun, S. De, I. T. McGovern, B. Holland, M. Byrne, Y. K. Gun'ko, J. J. Boland, P. Niraj, G. Duesberg, S. Krishnamurthy, R. Goodhue, J. Hutchison, V. Scardaci, A. C. Ferrari, J. N. Coleman, *Nat. Nanotechnol.* **2008**, *3*, 563.
[8] K. S. Novoselov, D. Jiang, F. Schedin, T. J. Booth, V. V. Khotkevich, S. V. Morozov, A. K. Geim, *Proc. Natl. Acad. Sci. USA* **2005**, *102*, 10451.
[9] S. S. Datta, D. R. Strachan, S. M. Khamis, A. T. C. Johnson, *Nano Lett.* **2008**, *8*, 1912.
[10] T. Wassmann, A. P. Seitsonen, A. M. Saitta, M. Lazzeri, F. Mauri, *Phys. Rev. Lett.* **2008**, *101*, 096402.
[11] A. Mañanes, F. Duque, A. Ayuela, M. J. López, J. A. Alonso, *Phys. Rev. B* **2008**, *78*, 035432.
[12] S. Adam, S. Cho, M. S. Fuhrer, S. Das Sarma, *Phys. Rev. Lett.* **2008**, *101*, 046404.
[13] N. Nemec, D. Tománek, G. Cuniberti, *Phys. Rev. B* **2008**, *77*, 125420.
[14] M. Y. Han, B. Ozyilmaz, Y. B. Zhang, P. Kim, *Phys. Rev. Lett.* **2007**, *98*, 206805.
[15] Z. H. Chen, Y. M. Lin, M. J. Rooks, P. Avouris, *Physica E* **2007**, *40*, 228.
[16] J. F. Dayen, A. Mahmood, D. S. Golubev, I. Roch-Jeune, P. Salles, E. Dujardin, *Small* **2008**, *4*, 716.
[17] X. L. Li, X. R. Wang, L. Zhang, S. W. Lee, H. J. Dai, *Science* **2008**, *319*, 1229.
[18] X. R. Wang, Y. J. Ouyang, X. L. Li, H. L. Wang, J. Guo, H. J. Dai, *Phys. Rev. Lett.* **2008**, *100*, 206803.
[19] X. Y. Yang, X. Dou, A. Rouhanipour, L. J. Zhi, H. J. Rader, K. Mullen, *J. Am. Chem. Soc.* **2008**, *130*, 4216.
[20] L. Zhi, K. Müllen, *J. Mater. Chem.* **2008**, *18*, 1472.
[21] K. S. Novoselov, A. K. Geim, S. V. Morozov, D. Jiang, Y. Zhang, S. V. Dubonos, I. V. Grigorieva, A. A. Firsov, *Science* **2004**, *306*, 666.
[22] K. S. Novoselov, A. K. Geim, S. V. Morozov, D. Jiang, M. I. Katsnelson, I. V. Grigorieva, S. V. Dubonos, A. A. Firsov, *Nature* **2005**, *438*, 197.
[23] M. L. Sadowski, G. Martinez, M. Potemski, C. Berger, W. A. de Heer, *Phys. Rev. Lett.* **2006**, *97*, 266405.
[24] K. S. Novoselov, Z. Jiang, Y. Zhang, S. V. Morozov, H. L. Stormer, U. Zeitler, J. C. Maan, G. S. Boebinger, P. Kim, A. K. Geim, *Science* **2007**, *315*, 5817.
[25] Y. W. Son, M. L. Cohen, S. G. Louie, *Phys. Rev. Lett.* **2006**, *97*, 216803.
[26] J. Moser, A. Barreiro, A. Bachtold, *Appl. Phys. Lett.* **2007**, *91*, 163513.
[27] M. Ishigami, J. H. Chen, W. G. Cullen, M. S. Fuhrer, E. D. Williams, *Nano Lett.* **2007**, *7*, 1643.
[28] M. A. Meitl, Z. T. Zhu, V. Kumar, K. J. Lee, X. Feng, Y. Y. Huang, I. Adesida, R. G. Nuzzo, J. A. Rogers, *Nat. Mater.* **2006**, *5*, 33.
[29] P. Blake, E. W. Hill, A. H. C. Neto, K. S. Novoselov, D. Jiang, R. Yang, T. J. Booth, A. K. Geim, *Appl. Phys. Lett.* **2007**, *91*, 3124.
[30] J. S. Villarrubia, *J. Res. Natl. Inst. Stand. Technol.* **1997**, *102*, 425.
[31] P. J. de Pablo, C. Gomez-Navarro, J. Colchero, P. A. Serena, J. Gomez-Herrero, A. M. Baro, *Phys. Rev. Lett.* **2002**, *88*, 36804.
[32] C. Gomez-Navarro, P. J. de Pablo, J. Gomez-Herrero, *Adv. Mater.* **2004**, *16*, 549.
[33] J. Y. Park, S. Rosenblatt, Y. Yaish, V. Sazonova, H. Ustunel, S. Braig, T. A. Arias, P. W. Brouwer, P. L. McEuen, *Nano Lett.* **2004**, *4*, 517.
[34] M. S. Purewal, B. H. Hong, A. Ravi, B. Chandra, J. Hone, P. Kim, *Phys. Rev. Lett.* **2007**, *98*, 186808.
[35] P. Sundqvist, F. J. Garcia-Vidal, F. Flores, M. Moreno-Moreno, C. Gomez-Navarro, J. S. Bunch, J. Gomez-Herrero, *Nano Lett.* **2007**, *7*, 2568.
[36] R. R. Haering, P. R. Wallace, *J. Phys. Chem. Solids* **1957**, *3*, 253.
[37] A. H. Castro Neto, F. Guinea, N. M. R. Peres, K.S. Novoselov, A. K. Geim, **2007**, http://arxiv.org/abs/0709.1163v1.
[38] This relatively low value of the mobility might be dominated by graphene–substrate interactions.
[39] Y. W. Son, M. L. Cohen, S. G. Louie, *Nature* **2006**, *444*, 347.

Received: October 1, 2008
Revised: December 9, 2008
Published online: February 25, 2009